Magnetospheric feedback in solar wind energy transfer

M. Palmroth,[1] H. E. J. Koskinen,[1,2] T. I. Pulkkinen,[1] P. K. Toivanen,[1] P. Janhunen,[1] S. E. Milan,[3] and M. Lester[3]

Received 31 May 2010; revised 31 August 2010; accepted 7 September 2010; published 11 December 2010.

[1] The solar wind kinetic energy fueling all dynamical processes within the near-Earth space is extracted in a dynamo process at the magnetopause. This direct energy transfer from the solar wind into the magnetosphere depends on the orientation of the interplanetary magnetic field (IMF) as well as other solar wind parameters, such as the IMF magnitude and solar wind velocity. Using the GUMICS-4 magnetohydrodynamic (MHD) simulation, we find that the energy input from the solar wind into the magnetosphere depends on this direct driving as well as the magnetopause magnetic properties and their time history in such a way that the energy transfer can continue even after the direct driving conditions turned unfavorable. Such a hysteresis effect introduces discrepancies between the energy input proxies and the energy input measured from GUMICS-4, especially after strong driving, although otherwise the simulation energy input captures the system dynamics. For the cause of the effect, we propose a simple feedback mechanism based on magnetic flux accumulation in the tail lobes. By ideal MHD theory, the energy conversion at the magnetopause is proportional to the product of normal and tangential magnetic fields, the magnetic stress. During large magnetic flux accumulation, the tangential field at the magnetopause strengthens, enhancing the local instantaneous energy conversion and transfer. Our simulations show that this mechanism supports the energy transfer even under weak driving followed by favorable solar wind conditions and transfer up to 50% more power than without the feedback.

Citation: Palmroth, M., H. E. J. Koskinen, T. I. Pulkkinen, P. K. Toivanen, P. Janhunen, S. E. Milan, and M. Lester (2010), Magnetospheric feedback in solar wind energy transfer, *J. Geophys. Res.*, *115*, A00I10, doi:10.1029/2010JA015746.

1. Introduction

[2] The solar wind energy transfer to the Earth's magnetosphere is a central issue in space physics, from both technological and scientific viewpoints: It is the cause of space weather phenomena, and the system energetics must be known to predict the system behavior under varying conditions. The direct energy transfer is assumed to have two components enabled by viscous interactions at the magnetopause [*Axford and Hines*, 1961] and reconnection between the interplanetary magnetic field (IMF) and the dayside terrestrial magnetic field [*Dungey*, 1961]. From these two, reconnection is believed to have a more significant role, as, for example, the polar cap potential (produced by the solar wind and magnetosphere coupling) reduces to low values during inefficient dayside reconnection [*Reiff et al.*, 1981]. This paper investigates the energy transfer as a consequence of the magnetopause reconnection.

[3] Figure 1 is a schematic of the energy transfer enabled by dayside reconnection. In Figure 1a, the southward IMF and the northward terrestrial magnetic field reconnect, creating open field lines that advect tailward on the magnetopause surface with the solar wind flow. In the tail, the open field lines are added to the tail lobes until tail reconnection closes them and they return back to the dayside [*Dungey*, 1961; *Milan et al.*, 2007]. The process may be viewed as an energy conversion system [*Siscoe and Cummings*, 1969; *Lundin and Evans*, 1985], where the dayside is a load while the nightside magnetopause is a generator (Figure 1a). The load converts magnetic energy into kinetic energy, while the opened field lines advecting tailward are pushed by the solar wind flow, and the tail magnetic energy density increases at the expense of solar wind kinetic energy. During northward IMF (Figure 1b), the lobe reconnection gives rise to sunward convection, while large parts of the tail magnetosphere are stagnant.

[4] The energy conversion is measured as the divergence of the Poynting vector $\mathbf{S} = (1/\mu_0)\mathbf{E} \times \mathbf{B}$, where $\mathbf{E}$ is the electric field, $\mathbf{B}$ is the magnetic field, and μ_0 is the vacuum permeability. In the time-independent case, $\nabla \cdot \mathbf{S} = -\mathbf{E} \cdot \mathbf{J}$, where $\mathbf{J}$ is the current density. During southward IMF, $\mathbf{E} \cdot \mathbf{J} > 0$ in the dayside load, while $\mathbf{E} \cdot \mathbf{J} < 0$ in the nightside generator. The signs of $\mathbf{E} \cdot \mathbf{J}$ arise from the direction of magnetopause Chapman-Ferraro currents (J_{MP} in Figure 1) and the advection direction of the open field lines. During northward IMF (Figure 1b), the generator

[1]Finnish Meteorological Institute, Helsinki, Finland.
[2]Also at University of Helsinki, Helsinki, Finland.
[3]Department of Physics and Astronomy, University of Leicester, Leicester, UK.

0148-0227/10/2010JA015746

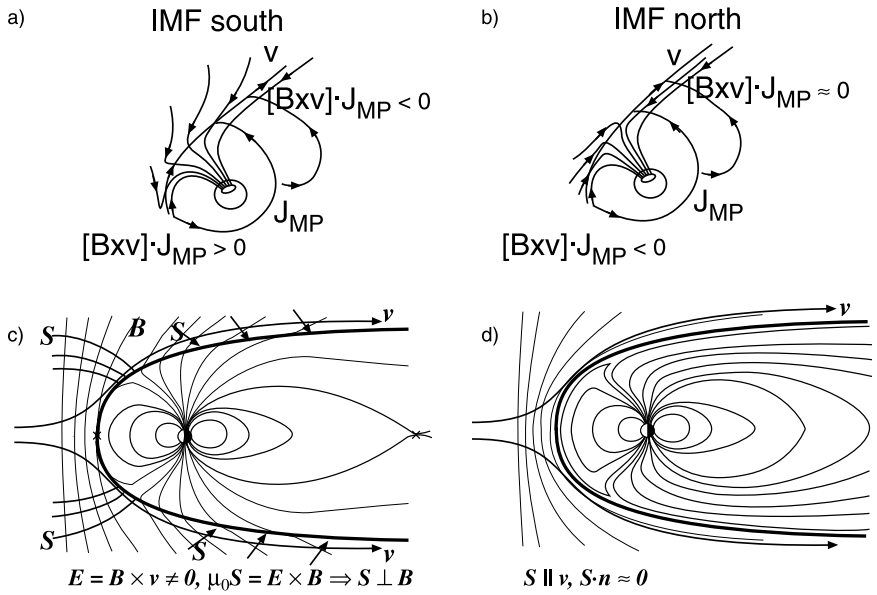

Figure 1. Schematic view of the magnetopause energy transfer in view of the load and dynamo process during (a) southward IMF, and (b) northward IMF. Poynting flux focusing during (c) southward IMF and (d) northward IMF. See text for details.

region can exist on the dayside ($\mathbf{E} \cdot \mathbf{J} < 0$), while on the nightside magnetopause $\mathbf{E} \cdot \mathbf{J} \approx 0$ except close to a possible lobe reconnection region. In the dynamo process, it is in fact the magnetic stress at the magnetopause that extracts solar wind flow energy to magnetic energy in the magnetosphere [*Siscoe and Cummings*, 1969]. The magnitude of the surface magnetic stress T is given by the following:

$$T = \frac{B_n B_t}{\mu_0} \tag{1}$$

where B_n and B_t are the normal and tangential magnetic fields at the magnetopause.

[5] The energy transfer process can also be viewed in terms of Poynting flux focusing [*Papadopoulos et al.*, 1999; *Palmroth et al.*, 2003], shown in Figure 1c. The tailward advecting open field lines give rise to a normal component of the magnetic field through the magnetopause, implying a nonzero component of the Poynting vector across the magnetopause. *Papadopoulos et al.* [1999] illustrated the consequence of the definition of the Poynting vector in the global simulation setup: The direction of the Poynting vector is aligned with the solar wind flow, but it starts to bend at the bow shock and focus toward the magnetopause. While in Figure 1c we only draw a few arrows showing the Poynting vector direction to avoid too many lines in the same figure, the Poynting flux crosses the magnetopause and focuses toward the tail reconnection region, from where it flows both toward and away from the Earth. The focusing occurs in the plane of the IMF, while the flow lines deviate away from the magnetopause in the plane perpendicular to the IMF direction. During northward IMF (Figure 1d), the magnetic field lines do not have a normal component through the tail magnetopause. Instead, the Poynting vector is parallel to the magnetosheath velocity $\mathbf{v}$ over the entire closed magnetopause, while small focusing can occur in the dayside due to lobe reconnection and sunward convection. The total power P transferred through the surface A is given by the following:

$$P = \int_A \mathbf{S} \cdot \mathbf{dA} \tag{2}$$

As the tangential component of the electric field is $E_t = vB_n$ at the magnetopause, Poynting flux focusing can be related with the dynamo process, because

$$P = \int_A S_n dA = \int_A \frac{B_t E_t}{\mu_0} dA = \int_A v \frac{B_n B_t}{\mu_0} dA, \tag{3}$$

where the magnitudes are given in the frame normal (subscript n) and tangential (subscript t) to the magnetopause, and the power is given in watts.

[6] While above we describe the direct energy transfer through the magnetopause, the energy transfer and dissipation often occur in a loading-unloading cycle, the substorm [*Rostoker et al.*, 1987; *McPherron*, 1991]. The lobe magnetic energy density first increases due to the dynamo process, and the tail stretches during the substorm growth phase. The antiparallel open magnetic fluxes from the two hemispheres meet again in the tail, and after some time, they reconnect, forming closed flux that returns to the dayside. Essentially, during the expansion phase and the subsequent recovery, the previously loaded energy is dissipated in the ionosphere and manifested in auroral displays and enhanced ionospheric currents. The loading-unloading cycle thus introduces a time delay between the direct energy transfer and the dissipation within the magnetosphere and ionosphere.

[7] As the energy transfer is difficult to quantify observationally on the vast magnetopause, it has been assessed by

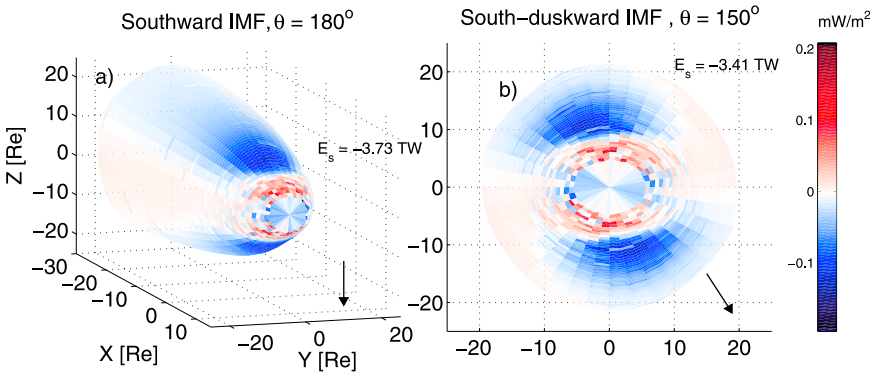

Figure 2. Example of the energy transfer computation using the GUMICS-4 simulation for (a) southward IMF viewed from the dawn flank and for (b) IMF $\theta = 150°$ viewed from the front looking tailward. The IMF orientation is shown by a black arrow in the lower right corner. Shown is the magnetopause surface identified using the streamline method [*Palmroth et al.*, 2003], and color-coded is the amount of incident energy on the surface (the integrand of equation (4)). Since the surface normal is positive outward, the inward energy flux is negative (blue), while outflowing energy from the dayside reconnection region is positive (red). The total amount of transferred energy (E_s) is shown on each graph.

correlation analyses of solar wind parameters and magnetic activity indices [e.g., *Akasofu*, 1981; *Newell et al.*, 2007]. These proxies of energy transfer typically include the solar wind speed, IMF magnitude, IMF clock angle in the YZ plane $\theta = \tan^{-1}(IMF_y/IMF_z)$, and sometimes the solar wind density. Perhaps the most widely known proxy for energy transfer is the ϵ parameter [*Akasofu*, 1981], whose functional form resembles electromagnetic Poynting flux incident on an area upstream of the Earth. Also, global magnetohydrodynamic (MHD) simulations have been used to directly evaluate the amount of energy transfer at the magnetopause, and the results on the total amount of incident energy on the magnetopause agree to a large extent with the observation-based proxies [*Palmroth et al.*, 2003, 2006a]. Furthermore, the simulated magnetopause reconnection and the load and dynamo processes agree with theoretical work [*Laitinen et al.*, 2007, and references therein]. Recent in situ measurements of the local energy conversion rates at the magnetopause are in quantitative accordance with the simulation results [*Rosenqvist et al.*, 2008].

[8] *Palmroth et al.* [2006b] investigated the clock angle dependence of the global energy transfer using a global MHD simulation GUMICS-4 [*Janhunen*, 1996] and found a hysteresis effect, indicating that the energy transfer can remain at a high level after large energy input, although the driver becomes weaker. While the mechanism causing the hysteresis was not identified, *Palmroth et al.* [2006b] showed that the effect was not due to the numerics within the simulation or in the method of computing the total energy transfer. A hysteresis has also been found in another simulation (a three-dimensional particle simulation), where the dayside magnetopause standoff distance responds hysteretically for changing IMF [*Cai et al.*, 2009]. However, the cause of the hysteresis has remained unknown.

[9] Here, we first review the main methodology to investigate the energy transfer using the GUMICS-4 global MHD simulation. Then we describe the hysteresis effect in several simulation runs. As a clear distinction from *Palmroth et al.* [2006b], we now propose a mechanism for the hysteresis arising from open magnetic flux accumulation at the tail lobes and its role in sustaining the energy input.

2. Methodology

[10] GUMICS-4 is a state-of-the-art global MHD simulation whose performance has been extensively tested against observations [e.g., *Palmroth et al.*, 2003; *Pulkkinen et al.*, 2006]. GUMICS-4 solves the fully conservative MHD equations within the magnetosphere and is coupled with an electrostatic ionosphere by field-aligned currents, electron precipitation, and electric potential. Solar wind density, velocity, temperature, and magnetic field are given as input to the code (either from actual observations or using artificial input parameters), while a variety of quantities are given as an output of the computation in space and time within the simulation box extending from +32 R_E to −224 R_E in the x-direction and ±64 R_E in the $y - z$ directions.

[11] *Palmroth et al.* [2003] introduced a method with which the global energy transfer can be investigated using the GUMICS-4 simulation. First, the magnetopause boundary was identified from each file generated by GUMICS-4 by following a large number of streamlines from the upstream until −30 R_E in the tail. The streamlines encompass the magnetosphere and form a cavity in the solar wind; the boundary of the cavity is then defined as the magnetopause surface. The magnetopause surface was found to coincide with the spatial gradients existing at the magnetopause; however, it is smoother than a surface based on plasma or current density gradients. The streamline magnetopause coincides with the statistical magnetopause location [*Shue et al.*, 1997, 1998], and the magnetopause search method has also been found to work in *Shukhtina et al.* [2009] using the OpenGGCM global MHD simulation [e.g., *Raeder*, 2003].

Table 1. Runs in *Palmroth et al.* [2006b]

Run #	|IMF| (nT)	SW Speed (km/s)[a]	SW Density (1/cm^3)	Dynamic Pressure (nPa)	Delay (min)
1	5	400	7.3	2	30
2	10	400	7.3	2	40
3	5	600	13.3	8	20
4	10	600	13.3	8	30

[a]SW, solar wind.

[12] The total energy perpendicular to the magnetopause boundary was defined as the portion of energy entering the magnetopause as follows:

$$E_s = \int_A \mathbf{K} \cdot \mathbf{n} dA \approx \int_A \mathbf{S} \cdot \mathbf{n} dA, \quad (4)$$

where **K** is the total energy density (kinetic + thermal + electromagnetic) in the GUMICS-4 simulation calculated at the surface of the magnetopause, **n** is the unit normal vector of the surface pointing outward, and dA is the area of the surface element. The right-hand side of equation (4) represents the fact that in the simulation, the electromagnetic energy constitutes the major portion of the total energy input, usually more than 95% [*Palmroth et al.*, 2006b]. The computation requires that the surface is identified for each time instant. The integration proceeds from the nose to −30 R_E in the tail.

[13] Figure 2 presents examples of the identified surfaces with color coding of the incident energy on the surfaces. The time instants are taken from a simulation run that is explained in detail in section 3. Blue (and negative) areas show the inward energy flux at the magnetopause, while red (positive) is the outward energy at the dayside reconnection region. Figure 2 illustrates clearly the quality of the magnetopause detection method, as the surface is smooth, having no irregularities in the orientation that might affect the computation of equation (4). For southward IMF (Figure 2a), the main areas of energy inflow are the northern and southern tail lobes, and the maximum energy transfer takes place from the terminator to approximately −10 R_E. The dayside reconnection region shows as energy outflow. As the inflow areas are larger than the outflow areas, the total energy transfer rate is −3.7 TW inward. For south-duskward IMF (θ = 150°; Figure 2b), however, the energy transfer location has tilted from the pure north-south direction. Figure 2b illustrates nicely the property of the Poynting vector, which focuses toward the magnetopause in the plane of the IMF and deviates away from the magnetopause in the plane perpendicular to the IMF. This originates from the fact that the open field lines advect tailward in the plane of the IMF, as also predicted by theoretical models [e.g., *Cooling et al.*, 2001].

3. Hysteresis in Magnetopause Energy Transfer

[14] In this section, we present several simulation runs showing the hysteresis originally identified by *Palmroth et al.* [2006b]. We begin by briefly reviewing the essential parts of this paper.

3.1. Description of the Hysteresis

[15] To study the clock angle and solar wind dynamic pressure dependence of the total energy transfer, the runs specified in Table 1 were carried out. In each run, the IMF rotated in the $y - z$ plane from the north (θ = 0°) via dusk (θ = 90°) to south (θ = 180°) and dawn (θ = 270°) and finally back to the north with 10° steps. Each clock angle value was kept constant for 10 minutes, and the run corresponds to 6 hours in real time. In each run, the other solar wind input parameters given in Table 1 were constant during the run.

[16] Figure 3 shows the results of the energy transfer through the magnetopause in Run 2. While the data shown here are taken from Figure 1 of *Palmroth et al.* [2006a], we have switched the negative sign of total energy through the magnetopause to positive and added more illustrations to better display the hysteresis pattern. Shown in Figure 3a is the total integral of the energy transfer against the IMF clock angle θ, where angles from 0° to 180° are given in the bottom horizontal axis and angles >180° on the top axis. Figures 3b–3f are instantaneous azimuthal integrals of energy transfer shown as polar histograms in the $y - z$ plane. The distributions are produced by integrating the energy transfer from nose to −30 R_E in six 60° wide sectors normalized to the outer circle (1500 GW). Figure 3b is the same

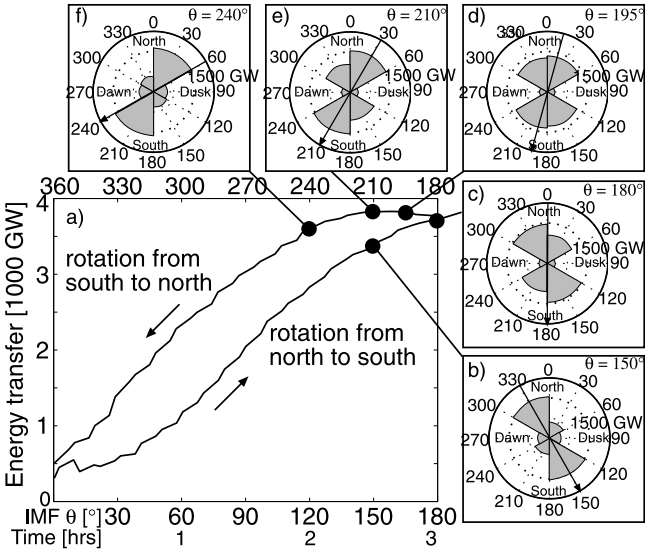

Figure 3. (a) Total energy transfer through the magnetopause against the IMF θ, angles less than 180° on bottom axis, and angles larger than 180° on top axis. Small arrows give the direction of rotation. (b–f) Instantaneous distributions of energy transfer viewed from the front of the magnetopause at times indicated by a black dot in Figure 3a. Shaded areas show the amount of energy transfer normalized to 1500 GW at the outer circle. The black arrow is the direction of the IMF. The results are from Run 2 in Table 1.

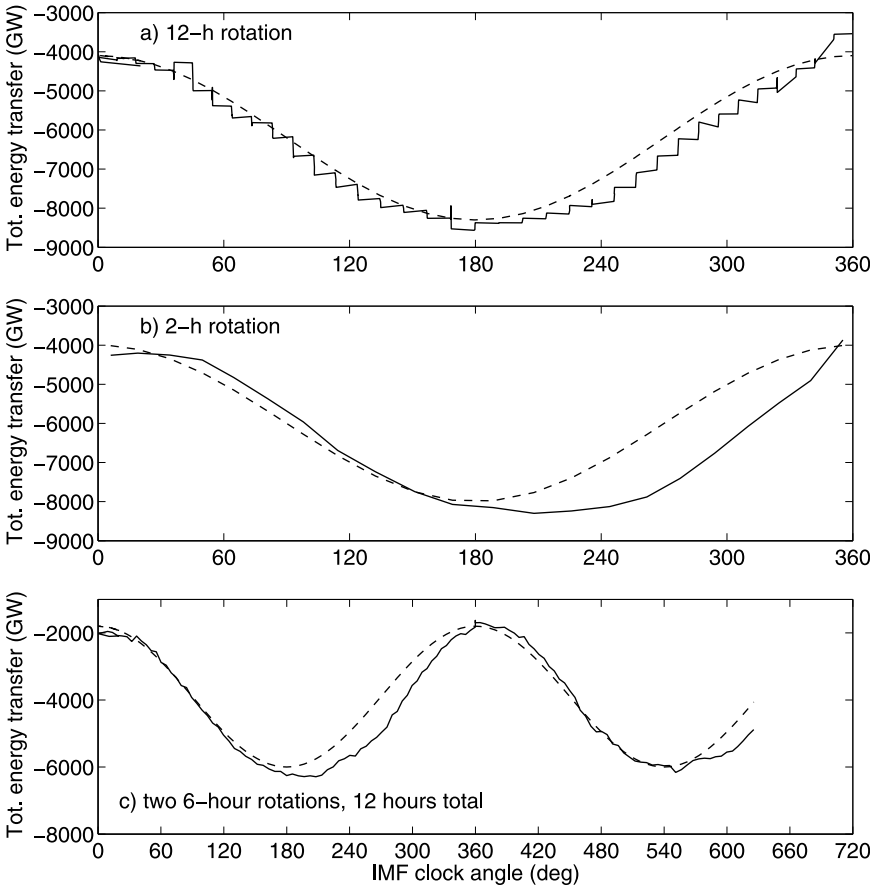

Figure 4. Total energy transfer in a run, where the IMF rotates (a) in 12 hours and (b) in 2 hours as compared to the runs rotated in 6 hours in Table 1. (c) Total energy transfer in a run with two consecutive rotations that take 6 hours each (12 hours in total). Solid line is the simulation result of the energy transfer, while the dashed line is the scaled $\sin^2(\theta/2)$ function computed from the upstream parameters at (18,0,0) R_E. The run in Figure 4c was carried out only until the hysteresis in the second rotation started to show (to save computation time).

time instant as given in Figure 2b, where the energy transfer results can be seen without the sector-wise integrals. The black arrow gives the IMF orientation for each image. The sectors with the longest bars show the sectors of largest energy input. A large sector in Figures 3b–3f hence indicates the area where field lines are advecting tailward, allowing Poynting flux focusing and energy transfer and conversion. Figure 3 shows that up to 50% more energy transfers during the return rotation as compared to the initial rotation, indicating a hysteresis as a function of θ. The extra energy during the return rotation comes from sectors that have transferred energy at earlier times; if no hysteresis were present, the energy transfer distributions in Figures 3b and 3e would be mirror images with respect to the north-south axis.

[17] *Palmroth et al.* [2006b] considered whether the phenomenon might originate from the numerics of the simulation, the method of computing the energy transfer, or the physics within the simulation. The simulation is strictly conservative, and hence no artificial energy can be left in the grid cells during the computation. The magnetic divergence is cleaned out every 20 seconds. The method used to compute the total transfer includes the identification of the magnetopause, which might have irregularities in the size or orientation. The total area is not larger during the south-to-north rotation as compared to north-to-south rotation, and hence the area is not the cause of the hysteresis. The orientation as a possible cause was investigated such that for each time instant, equation (4) was computed with the energy flux from the time instant in question, but through a surface switched about the symmetry time at $\theta = 180°$. This means that, for example, the value at $\theta = 150°$ in Figure 3b used the energy flux at $\theta = 150°$, but through a surface identified at $\theta = 210°$. The outcome of the test was identical to the original computation, and the orientation of the surface as a possible cause of the phenomenon was ruled out. Hence, *Palmroth et al.* [2006b] concluded that neither the simulation nor the energy calculation method causes the hysteresis, which must then be caused by the physics of the simulation. However, with regard to the main objective of the present paper, the mechanism for the hysteresis was not identified.

[18] *Palmroth et al.* [2006b] went on to quantify the effect by computing the time delay with which the return rotation energy transfer correlates best with $\sin^2(\theta/2)$, which was shown to best represent the energy transfer clock angle

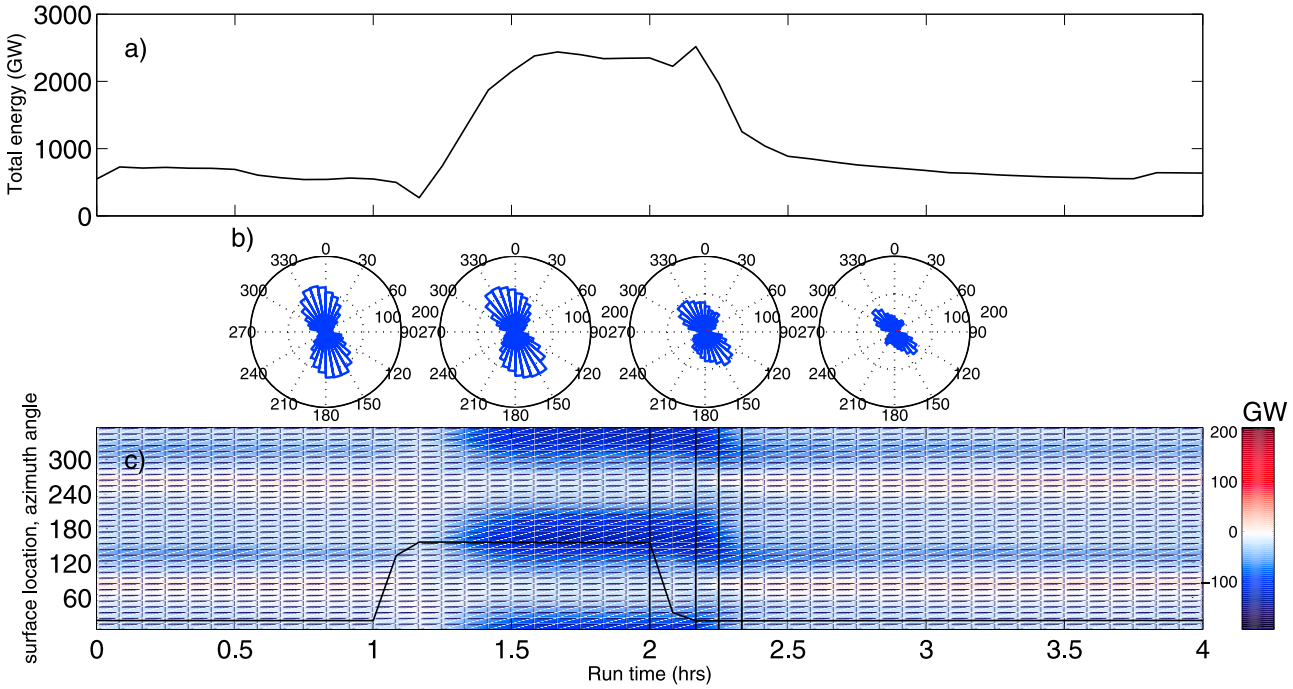

Figure 5. (a) Total energy transfer through the magnetopause against time in a run where the IMF flips from north to south and vice versa without changing the *y*-component while maintaining the same magnitude. (b) Instantaneous distributions of energy transfer viewed from the front of the magnetopause; the distributions are similar to those in Figures 3b–3f, but are plotted with finer angular resolution. (c) Sectorwise energy integrals against time in thirty-six 10° wide sectors. The instantaneous distributions in Figure 5b are given at the times shown by the vertical lines, while the black line denotes the IMF clock angle evolution in time. Blue indicates inward energy, and red is outward energy in Figures 5b and 5c.

variation. Table 1 shows this delay, which increases with large IMF magnitude and small dynamic pressure and shortens with large dynamic pressure and small IMF magnitude.

3.2. Results of Further Simulations

[19] Figure 4 shows the results on the energy transfer in runs having a 12-hour rotation (Figure 4a), a 2-hour rotation (Figure 4b), and a run with two 6-hour consecutive rotations (the total run time was 12 hours; Figure 4c). The other solar wind conditions in the runs in Figure 4 are the same as in Run 3 in Table 1 having the smallest hysteresis delay. Plotted is also the scaled $\sin^2(\theta/2)$ function for reference. While the hysteresis depends on the time rate of change, it is still clearly seen in all runs, although the rotation speed is different. In the 2-hour run, also the initial north-to-south rotation seems slightly delayed. Figure 4c shows that the northward IMF before the second rotation "cleans" the hysteresis, and the second north-to-south rotation occurs in concert with the $\sin^2(\theta/2)$ function. The run has been carried only until the hysteresis during the second rotation starts to show (to save computation time). The fact that the northward IMF cleans the hysteresis before the second rotation implies that there is nothing numerical (such as magnetic monopoles due to possibly inefficient cleaning of the magnetic field divergence) in the simulation that accumulates and causes the hysteresis, which further strengthens the conclusion that the cause of the effect is not in the simulation numerics. To further check the numerics, the runs in Figures 4a and 4b are carried out with a smaller spatial resolution than the run in Figure 4c. The amount of energy transfer in the runs in Figures 4a and 4b is almost identical, indicating that the simulation energy transfer is predictable with the same initial conditions, adding more confidence to the simulation numerics. The amount of total energy transfer is different in runs with different spatial resolution; this is due to the fact that the current density at the magnetopause computed from the magnetic field gradients is smaller in the runs having a larger grid size. However, as the hysteresis is present in all runs having different spatial resolution, we may conclude that the simulation numerics are likely not the cause of the effect.

[20] We also carried out a run with a counter-clock-angle-wise rotation (not shown), where the hysteresis was also visible. In fact, in this run, where IMF is rotated from dawn-south-dusk-north, the energy transfer distribution for θ = 210° is a mirror image of the distribution in Figure 3b, while the distribution for θ = 150° is a mirror image of the distribution in Figure 3e. Hence, generally, the sectors transferring energy during the return rotation are those that were transferring energy during the initial rotation, regardless of the direction of rotation. A run where the IMF returns back to north without changing the sign of the IMF_y component also contains the hysteresis, although the time delay is now slightly smaller than in the full rotations (not shown).

[21] Figure 5 shows results from a run having an instantaneous north-to-south flip in the IMF direction. In this run, the original IMF_y component and the IMF magnitude were

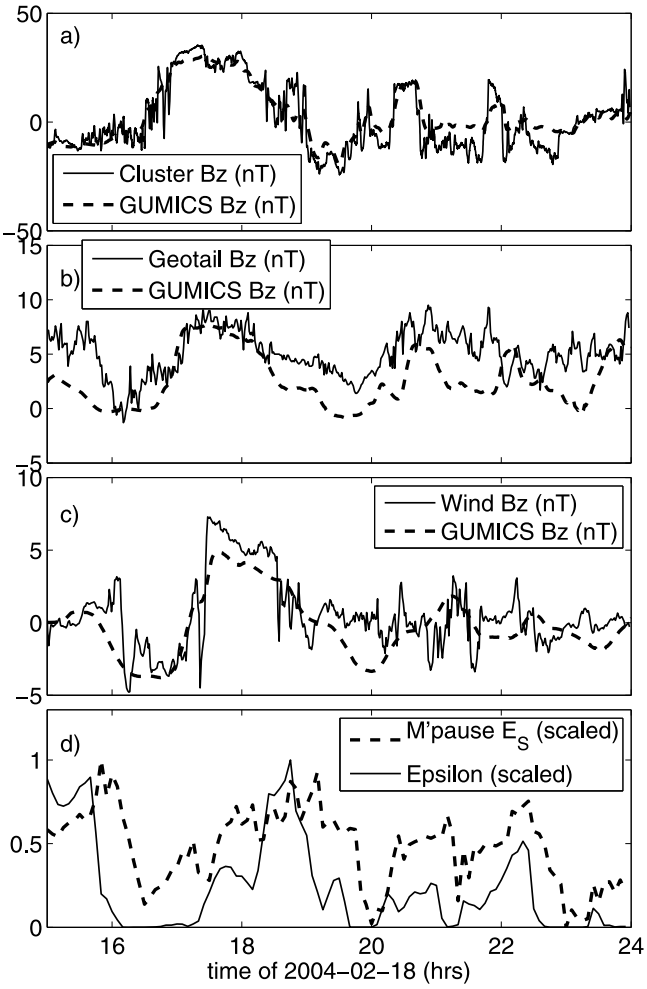

Figure 6. (a) Cluster observations of the dayside magnetosheath magnetic field z-component (solid black) on 18 February 2004 as recorded by the FGM instrument. The dashed black trace is the GUMICS-4 reproduction of the B_z component on Cluster orbit. (b) Geotail observations of the near-tail magnetic field z-component (black), and GUMICS-4 reproduction of B_z on Geotail orbit (dashed black). (c) Wind observations of the far-tail magnetic field z-component (black), and GUMICS-4 reproduction of B_z on Wind orbit (dashed black). All spacecraft data are interpolated to the same cadence that GUMICS data are saved. (d) The ϵ parameter computed from the actual upstream parameters delayed to the magnetopause (black) and scaled between 0 and 1. The dashed black trace is the GUMICS-4 result of the scaled energy transfer through the magnetopause.

not changed during the simulation period. The IMF clock angle is 20° before the flip, 160° during the flip, and at 2 o'clock run time (RT), the IMF flips back to 20°. Figure 5a gives the total energy transfer through the magnetopause, now plotted against time. Figure 5b shows similar sector-wise energy integrals as given in Figures 3b–3f, but plotted with a finer angular resolution as 36 sectors are illustrated (as compared to six sectors in Figures 3b–3f). The sector-wise integrals in Figure 5b are given at times shown as vertical lines in Figure 5c, which gives the time evolution of the sector-wise energy integral, where blue is inward energy and red outward. The same 36 sectors as those given in Figure 5b are color-coded for each time instant.

[22] Figure 5 clearly illustrates that the energy transfer remains at an elevated level for about 15 minutes after the IMF turns back to northward. This illustrates that the hysteresis is not only associated with the rate of change in the IMF and the IMF_y component, but is generally related to previous driving conditions. The sector-wise integrals in Figures 5b and 5c indicate that again the sectors contributing to energy transfer during southward IMF are aligned with the clock angle orientation. During northward IMF, there is faint energy outflow from the equatorial sectors (shown in red in Figures 5b and 5c). This is likely due to lobe reconnection and sunward convection. If the IMF clock angle flip is carried out from 20° to 200°, the results are otherwise the same as in Figure 5, but the sectors contributing to energy transfer during southward IMF are in the northern dusk and southern dawn, again aligned with the IMF orientation (not shown).

[23] In Figure 6, we show results from a simulation run where we use actual observed solar wind parameters recorded by the Advanced Composition Explorer (ACE) spacecraft as input to the simulation code. The event in question was recorded on 18 February 2004. During the event, the Cluster spacecraft were traversing the dayside magnetosheath, while Geotail traversed the near-tail at $X = -20\ R_E$ and flapped between the lobes and the plasma sheet. On the other hand, wind traversed the far-tail plasma sheet at $X = -130\ R_E$. Figures 6a–6c show the z-component of the magnetic field recordings onboard Cluster (FGM, [*Balogh et al.*, 2001]; Geotail (MGF, [*Kokubun et al.*, 1994]); and Wind (MFI, [*Lepping et al.*, 1995]). Overlaid with the spacecraft recordings are the GUMICS-4 reproduction of the B_z component on each of the spacecraft orbits. Overall, the GUMICS reproduction of the in situ measurements is good: The Cluster observations show almost one-to-one correspondence within the dayside magnetosheath, except for two intervals (at 2050–2145 UT and 2210–2255 UT), when the Cluster orbit in the simulation is outside the bow shock while in reality Cluster remains within the magnetosheath. The GUMICS reproduction of the Geotail magnetic field is fairly good, and the wind reproduction is exceptionally good when taking into account that owing to the adaptive gridding used in the simulation, the far-tail resolution is coarser than at the other two spacecraft orbits. While we only show the B_z comparisons to avoid too many curves in the same plot, other parameters are also well in accordance with the spacecraft recordings (not shown). Hence, we deduce that during the event in question, GUMICS-4 reproduces the in situ spacecraft observations, indicating that the simulation results can be interpreted in light of physical processes within the magnetosphere.

[24] Figure 6d shows the ϵ parameter computed using the upstream solar wind parameters and delayed to the magnetopause. The delay time has been calculated by correlating the upstream solar wind recordings (provided by ACE spacecraft) with the Cluster 1 magnetic field measurements in the magnetosheath, as well as using a distinct pressure pulse that compressed the dayside magnetic field recorded by GOES-12 (Honkonen et al., On large plasmoid formation in a global magnetohydrodynamic simulation, manuscript

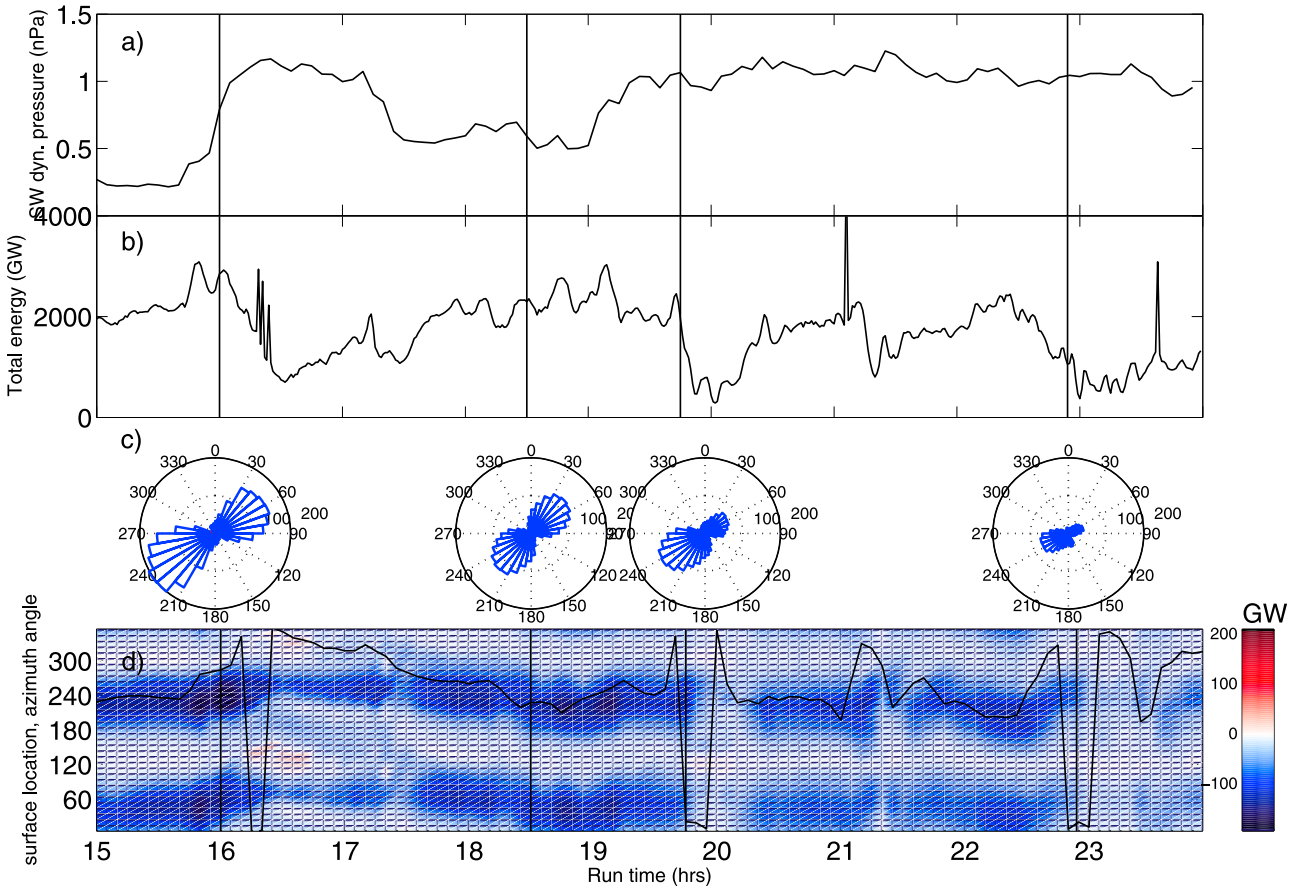

Figure 7. (a) Solar wind dynamic pressure just upstream of the bow shock in the simulation; the original data used as input to the simulation was recorded by ACE spacecraft on 18 February 2004. (b) GUMICS-4 results on total energy transfer during the 18 February 2004 event. (c) Instantaneous distributions of energy transfer viewed from the front of the magnetopause at times indicated by a vertical line in (d), where sector-wise energy integrals against time in 36 10° wide sectors are given. Overlaid in Figure 7d is also the IMF clock angle (black line) against time.

submitted to *Annales Geophysicae*, 2010). Both correlations yielded an unambiguous time delay of 46 minutes from the ACE position to the magnetopause. Depicted in Figure 6d is also the GUMICS-4 result on total energy transfer through the magnetopause. As can be seen, the simulation energy transfer increases in concert with the ϵ parameter, but stays enhanced for a while even though the ϵ decreases.

[25] Figure 7 gives the solar wind dynamic pressure, the total energy transfer in the simulation, and the sector-wise integrals (similar to Figures 5b and 5c) for the 18 February 2004 event. Figure 7 again illustrates that the energy transfer takes place in sectors aligned with the IMF orientation (first, second, and third vertical lines in Figures 7c and 7d). Again, the energy transfer stays enhanced for about 15 minutes after the clock angle turns northward (third vertical line in Figures 7c and 7d). The decrease of the energy transfer starts from the northern sectors (third and fourth vertical lines in Figures 7c and 7d), while the southern sectors still transfer energy. This is likely due to a constant positive IMF_x component during the event, which brings the IMF field lines better in contact with the southern hemispheric terrestrial field, thus favoring reconnection there. Also, the solar wind dynamic pressure jumps enhance the energy transfer, as can be seen, for instance, in the first vertical line in Figures 7c and 7d: The clock angle turns more northward while the dynamic pressure increases, enhancing also the energy transfer. On the basis of Figures 6 and 7, we conclude that the hysteresis is present also in this run, where the simulation reproduces in situ measurements.

4. On the Mechanism Behind the Hysteresis

[26] Although equation (3) says that the energy conversion rate at the magnetopause explicitly depends on the tangential magnetic field B_t, in practice the energy conversion has often been viewed as being dependent only on B_n, perhaps because the focus has been on dayside reconnection that creates the normal magnetic field component at the magnetopause. We now investigate the effect of the tangential field and get back to the IMF rotation runs where the hysteresis was first observed. Figure 8 shows the magnetopause normal magnetic field B_n, tangential magnetic field B_t, their product B_nB_t, and the azimuthal energy transfer for two time instants symmetrically distributed around $\theta = 180°$ in Run 2. The parameters B_n, B_t, and B_nB_t are evaluated on the magnetopause at the location of maximum energy

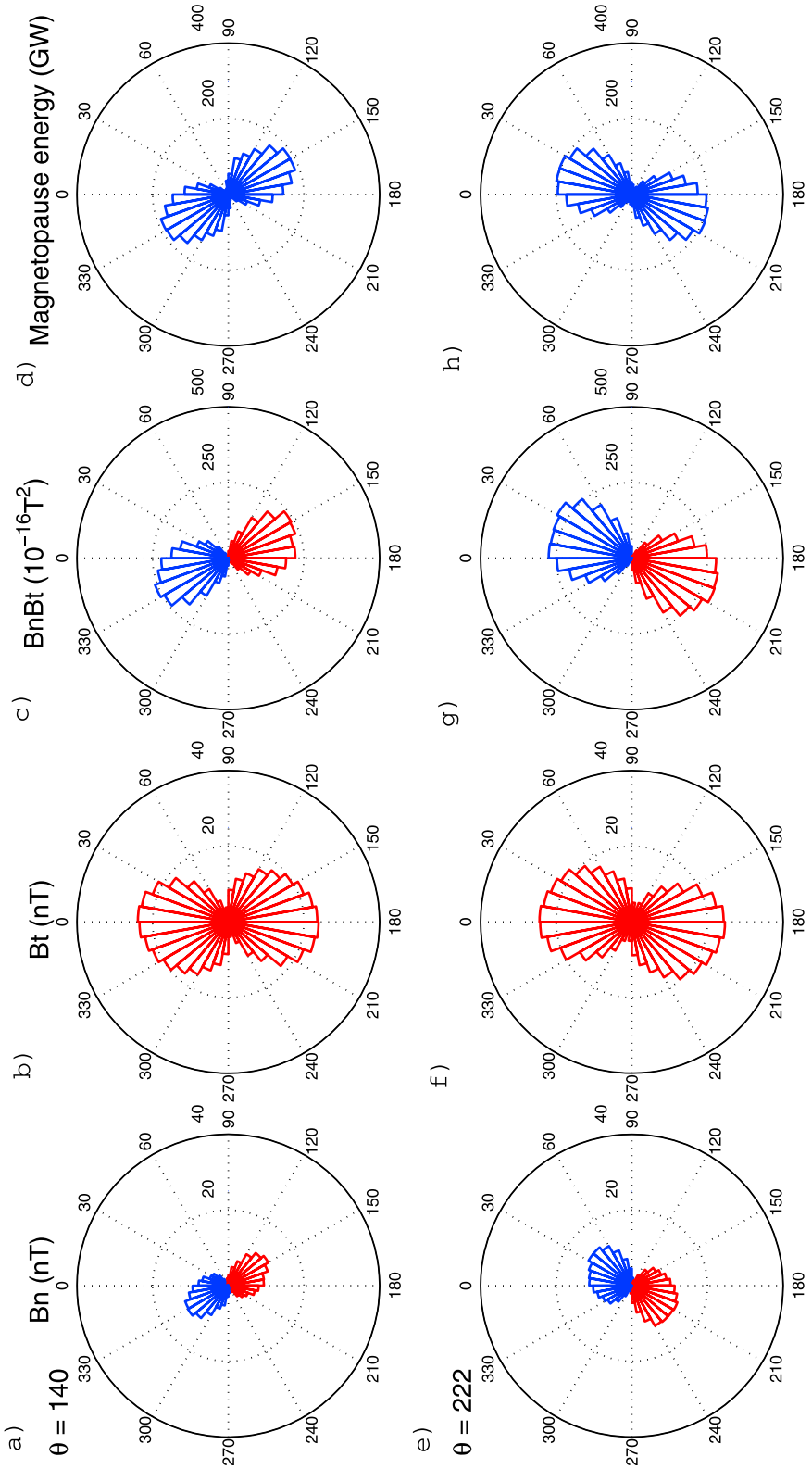

Figure 8. (a) Magnetopause normal magnetic field B_n, (b) tangential magnetic field B_t, (c) product B_nB_t, and (d) the azimuthal energy transfer distribution for Run 2 in Table 1 for IMF clock angle $\theta = 140°$. (e–h) The same parameters as for Figures 8a–8d, but for IMF clock angle $\theta = 220°$. Blue indicates negative values and red positive; scaling of the bars is given on the radial axis on the right of each diagram.

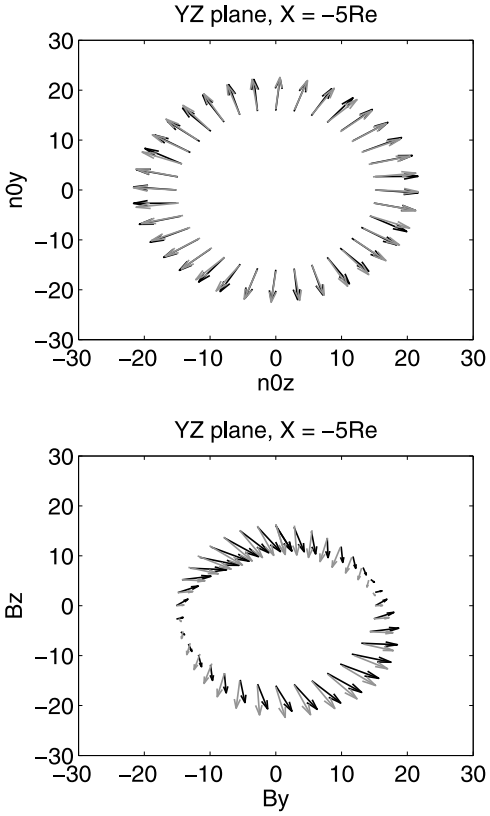

Figure 9. (top) Magnetopause normals (y- and z-components) in the $y - z$ plane at $x = -5\ R_E$. Black vectors are taken from time instant during which the IMF $\theta = 140°$, while gray vectors are those for $\theta = 220°$. (bottom) Magnetopause magnetic field (y- and z-components) in $y - z$ plane at $x = -5\ R_E$. The vectors for $\theta = 220°$ have been flipped with respect to the $x - z$ plane to take into account the different sign of IMF_y during the return rotation. Similar color-coding is used as in (a).

transfer rate at $X = -5\ R_E$ in the $y - z$ plane. Blue indicates negative values, and red positive (energy transfer is negative because the magnetopause normal vector points outward from the surface). The azimuthal energy transfer integrals in Figures 8d and 8h are produced similarly to the distributions in Figures 3, 5, and 7: by integrating the energy transfer over x values of the magnetopause in 36 10° wide sectors.

[27] The scaling of the bars is given on the radial axis on the right of each of the polar histogram plots, and the same scaling is used at both time instants (e.g., 40 nT for the B_n distribution). A large bar in each angular histogram in Figure 8 showing B_n, B_t, and B_nB_t means that the value for $B_n = \mathbf{B} \cdot \mathbf{n}$, $B_t = \mathbf{B} \cdot \mathbf{t}$, and B_nB_t is large on the magnetopause in $X = -5\ R_E$. This can originate from either **B** having larger values or being more perpendicular (or tangential) to the magnetopause. Figure 9 shows that the normals are exactly the same during the two time instants, while there is a difference in the magnetic field direction. The vectors for $\theta = 220°$ in Figure 9 (bottom) are mirrored with respect to the $x - z$ plane to take into account the different sign of IMF_y component during the return rotation.

[28] Figure 8 illustrates the origin of the above-stated observation that the extra energy during the return rotation comes from sectors that have transferred energy at earlier times (compare Figures 3b and 3e). During the initial north-to-south rotation before the IMF has visited due south, the energy transfer azimuthal distribution (Figure 8d) is skewed toward the northern dawn and southern dusk. However, during the return rotation south-to-north, the azimuthal distribution is less skewed and more aligned to the north-south axis (Figure 8h). This means that the rotation of the energy transfer distribution slows down after due south, and as a consequence some of the energy transfer still takes place in the northern dawn and southern dusk sectors that were mainly transferring energy before the IMF due south orientation.

[29] Comparing the B_n distributions in Figure 8 at both sides of due south, one can see that both during the north-to-south and south-to-north rotations, the B_n distributions are almost as skewed with respect of the north-south axis. The maxima of the distributions are in 330°–150° axis for $\theta = 140°$, and 30°–210° axis for $\theta = 220°$. This means that tailward advection of the newly opened field lines is tightly controlled by the IMF orientation, and the rotation of the distribution slows down only slightly. This indicates that the Cooling model [*Cooling et al.*, 2001] prediction of the dawn-dusk asymmetry in the advection of open flux tubes during finite IMF_y component is supported by these simulations.

[30] Figures 8b and 8f illustrate that the B_t distributions at $\theta = 140°$ and at $\theta = 220°$ are both essentially oriented toward the north-south axis. However, the B_t distribution shows slightly larger values at $\theta = 220°$. This is also true for the B_n distribution in Figure 8e. This means that the magnetic field accumulates in the tail (making **B** larger in $\mathbf{B} \cdot \mathbf{n}$ and $\mathbf{B} \cdot \mathbf{t}$). When the B_n and B_t distributions are multiplied, the larger B_t during the return rotation makes the product distribution less skewed. Ultimately, the cessation of the production of the new tailward advecting field lines, as well as tail reconnection and subsequent flux return to dayside, decrease the B_n and B_t distributions to the level they were at during the initial north-to-south rotation. Hence, the "cleaning" of the hysteresis occurs before the second rotation starts (Figure 4c).

[31] Figure 10 shows the B_n and B_t distributions for the run presented in Figure 5, where the IMF flips instantaneously at 0200 RT from $\theta = 160°$ back to $\theta = 20°$. Again, blue indicates negative values and red positive. Four time instants are given: immediately before the flip and 10, 15, and 20 minutes after the flip. Similarly to Figure 8, Figure 10 illustrates that the B_t distribution is aligned in the north-south direction during southward IMF, while the B_n distribution is aligned with the IMF orientation. After the flip, the B_t maintains its shape for 10 minutes before starting to reorganize (0215) for the northward IMF (0220), for which the B_t distribution is aligned in the dawn-dusk direction due to IMF draping over the closed magnetopause [*Kaymaz et al.*, 1992]. Figure 5, indicates that the energy transfer distribution maintains its general shape until 0215 RT, when the B_n distribution in Figure 10a is already disorganized and not aligned with the IMF orientation, i.e., showing the general signatures of the northward distribution. Hence, we deduce that at 0215, the shape of the energy transfer distribution must be maintained by the tangential field component.

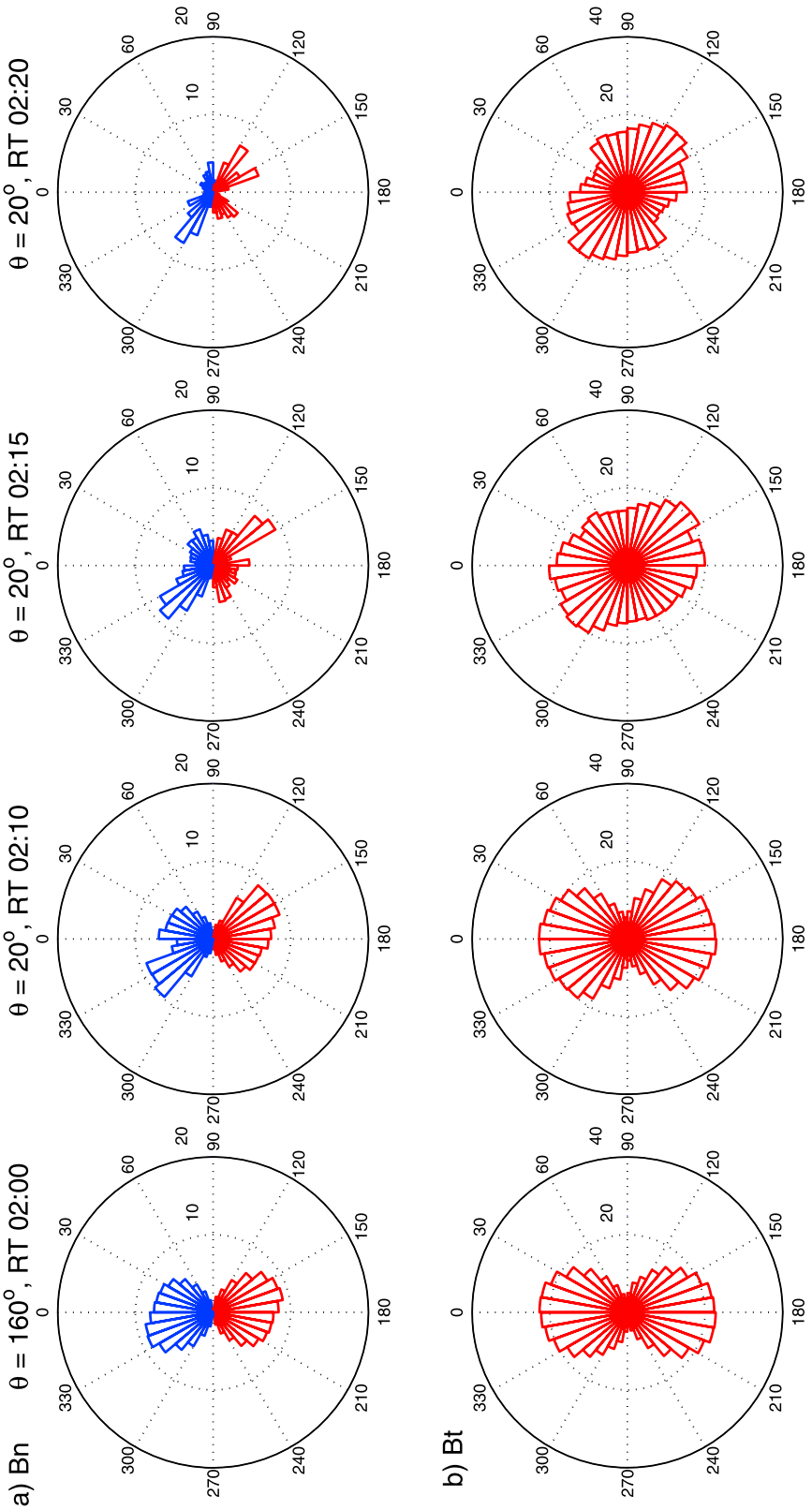

Figure 10. (a) B_n distribution at the magnetopause in $y-z$ plane, $x = -5\ R_E$, in a run where the IMF flips from north to south and vice versa without changing the y-component while maintaining the same magnitude. Four time instants are given: Run time (RT) 0200, 0210, 0215, and 0220. (b) The energy transfer distribution for the same time instants but depicted as the B_t distribution. Blue indicates negative values and red positive; scaling of the bars is given on the radial axis on the right of each diagram.

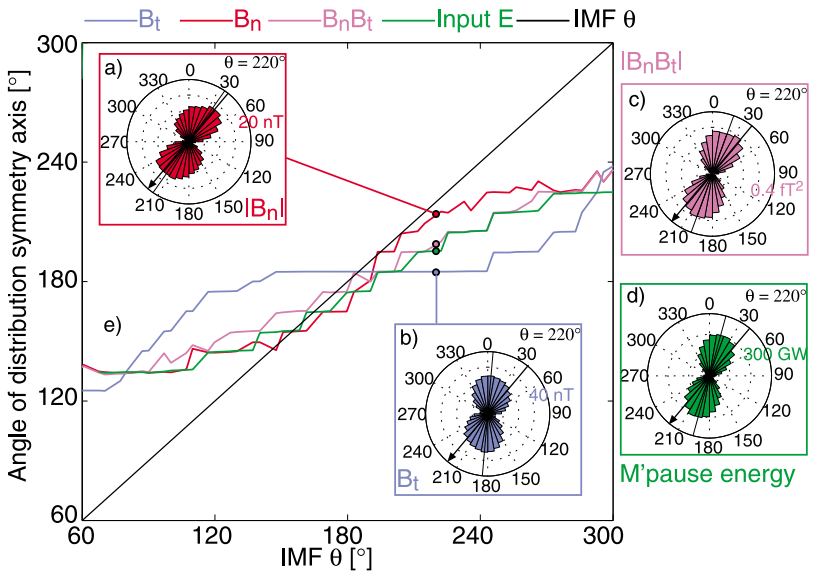

Figure 11. (a–d) Instantaneous distributions of magnetopause magnetic field in the normal (red) and tangential (blue) direction, their product (violet), and the energy transfer (green) at $\theta = 220°$. The black arrow in each diagram is the IMF orientation, while the thin black line is the axis of symmetry of the distribution. (e) Temporal evolution of the distribution skewness as given by the angle of each distribution symmetry axis with respect to north against IMF θ; the same colors are used to indicate different quantities as in Figures 11a–11d. The dots indicate the time and clock angle at which the instantaneous distributions in Figures 11a–11d are given.

[32] As a whole, Figure 8 illustrates that the energy transfer distribution looks most like the B_nB_t distribution, rather than like B_n or B_t alone. The product of the quickly rotating B_n and the slightly slower and increasing B_t rotates slower. This also holds for the other runs in Table 1 for all time instants. To check this quantitatively, we show in Figure 11 the temporal evolution of the skewness of each distribution. The colored areas of Figures 11a and 11b are the instantaneous polar histograms of B_n and B_t at a cross-section of the magnetopause in the $y - z$ plane at a location of largest energy transfer in the simulation magnetopause (at $x = -5\ R_E$). The distributions are given at $\theta = 220°$. The distribution for the product B_nB_t is given in Figure 11c, while Figure 11d gives the integrated energy transfer distribution (similar to Figures 3b–3f but with finer resolution). The thick black arrow is the IMF orientation, while the thin black line gives the axis at which the relative weights of the sectors are in balance. The angle of this symmetry axis is used to illustrate the temporal evolution of the distribution skewness and is given in Figure 11e. B_n is largely created between $60° < \theta < 300°$. For northward IMF, the B_n distribution is disorganized (cf. Figure 10a) and the angle of symmetry is not a useful parameter for describing the temporal evolution during northward IMF. Hence the horizontal axis is limited.

[33] Figure 11 shows that the B_n distribution is most skewed and best aligned with the IMF θ. When the open field lines advect to the tail, they become aligned with the magnetopause and strengthen the tangential field. Hence B_t is an accumulative quantity that changes slower than B_n; the distribution is aligned to the north-south orientation almost during the entire period of southward IMF. The energy transfer distribution mostly resembles the B_nB_t distribution, which is dominated by B_n when dayside reconnection is increasing and more field lines are opened but only a small amount of B_t has yet accumulated. While the dayside reconnection rate decreases during the return rotation, the tangential field still remains in the tail, dominating the B_nB_t distribution and maintaining the energy conversion at the magnetopause. The accumulation of tangential magnetic field and its role in the energy conversion also explains the extra energy coming from earlier energy transfer sectors as shown in Figure 3e.

[34] As shown in Table 1, the time delay of the simulation energy input with respect to $\sin^2(\theta/2)$ increases with increasing IMF magnitude and decreases with solar wind dynamic pressure (which was set up by increasing the solar wind speed and density together). Also, these pieces of evidence can be interpreted in light of the suggested mechanism. The larger the IMF magnitude, the faster the open magnetic field is created, while the larger solar wind speed increases the advection velocity. Hence, the IMF magnitude eventually brings more tangential field in the tail strengthening the hysteresis and the time delay, while the large advection speed quickly transfers the accumulated tangential field back to the dayside decreasing the tangential field. The individual distributions of B_n and B_t in several runs illustrate that for larger solar wind speed, the tangential field rotates quicker than in Figure 11e and hence contributes less to the energy conversion, decreasing the hysteresis effect.

5. Discussion

[35] In summary, we observe that in the GUMICS-4 simulation, the energy transfer stays enhanced longer than

predicted by present well-known energy transfer proxies, such as the ϵ parameter. This phenomenon that we name the *hysteresis* depends on the following parameters: the rate of change in the IMF, the dynamic pressure, the magnitude of the IMF, and possibly also whether there is a change in the IMF_y component (as the hysteresis time delay is larger for runs where the IMF_y changes). Our analysis suggests that the phenomenon is not caused by the numerical errors of the simulation or by the method of calculating the incoming energy, but is due to the physics within the simulation. On the basis of the results shown in this paper, the hysteresis can account for at least 50% of the incoming energy. Hence, the hysteresis can have a larger effect on the magnetospheric dynamics than, e.g., the viscous interactions that are estimated within the 10% level.

[36] Our simulation results are consistent with the ideal MHD theory prediction that the energy transfer is not only a function of the normal magnetic field at the magnetopause controlled by dayside reconnection and solar wind parameters, but it also depends on the tangential component of the magnetic field at the magnetopause. The tangential field is an accumulative quantity that can maintain the magnetopause energy transfer, regardless of direct driving, introducing a feedback between the energy transfer and the loading of the tangential field. The proposed mechanism is important to take into account in substorm studies, since particularly during the substorm growth phase, the open magnetic flux is accumulated in the tail [e.g., *McPherron*, 1991, and reference therein]. In fact, *Milan et al.* [2009] observed that substorms are more intense when more open magnetic flux has accumulated prior to onset. Such observations may also be explained in terms of our results, since with a large prior tangential field accumulation in the tail, also the instantaneous energy transfer at the magnetopause is larger.

[37] A classical substorm is thought to be a superposition of directly driven and loading-unloading components, as described, e.g., by *McPherron and Baker* [1993]. This means that the magnetospheric response to solar wind driving has two forms: one which is self-similar to the driver with a possible delay and one having previous loading and subsequent unloading components leading to a magnetospheric output unrelated to the temporal evolution of the input. The mutual effects of the components constitute the complicated evolution of the magnetospheric activity index in individual events. Here, we find that the actual energy transfer at the magnetopause (the physical input to the system) is possibly a superposition of two forms: one directly driven by the solar wind during the north-south rotation and the delayed component during the south-north rotation. This interpretation suggests that some of the time delays associated with substorms could be related to processes at the magnetopause.

[38] *McPherron et al.* [1988] employed a linear prediction filtering method to investigate the IMF control of the magnetic activity within the magnetosphere. They reported that "less than half the variance of the AL index is predictable by the solarwind," implying that both the dayside and nightside reconnection rates are delayed relative to the solar wind driving. In accordance with these findings, our results suggest that during the substorm growth phase, the energy transfer would depend also on the magnetic properties at the magnetopause, indicating a nonlinear response to the solar wind driving. Our results also show that the hysteresis is cleaned during northward IMF, suggesting that the magnetosphere would be more directly driven after long periods of northward IMF, and the nonlinearity in the solar wind-magnetosphere energy coupling would show after strong driving. The cleaning of the hysteresis is possibly related to the stagnant magnetospheric flows and the balance between the magnetic flux opening and closing rates during northward IMF, implying that the flux accumulation should be at minimum.

[39] The energy input proxies correlate with energy dissipation proxies, typically with a correlation coefficient less than 0.8 [*Newell et al.*, 2007], indicating that, e.g., ϵ does not always represent the system energetics. In a statistical investigation of 698 substorms, *Tanskanen et al.* [2002] found that the energy dissipation in the ionosphere is best correlated with the solar wind energy input as measured by the ϵ parameter during the substorm expansion phase, whereas the correlation between ϵ and the ionospheric dissipation is weaker during the entire substorm period. This indicates that the ϵ parameter is a good proxy for the system energetics after the release of the accumulated magnetic flux, while it does not represent the system energetics as well if the period of magnetic flux accumulation is also taken into the investigation. The mechanism for the hysteresis is consistent with these observations, because the energy input during times of a large amount of accumulated magnetic flux is not a function of solar wind parameters only, but also depends on the properties and time history of the magnetopause magnetic field.

[40] Because the in situ observations are essentially point measurements in the vast magnetosphere, the phenomenon has not been identified earlier when various energy transfer proxies have been developed. The simulations provide a global picture within which new global dependencies are more easily identified. The simulation-based proxies are generally in agreement with observation-based proxies [*Palmroth et al.*, 2004], and here we suggest that the new proxy for energy transfer should take into account the tangential field accumulation in the tail. While developing such a proxy is outside the scope of the present paper, we suggest that the new proxy could depend on prior amounts of energy transfer over a suitably chosen time interval. Experimentally, the hysteresis might be observable from large statistics of magnetospheric activity indices, with grouping according to prior history of IMF.

[41] **Acknowledgments.** We thank Kalle Pietilä for fruitful discussions. The Cluster data have been retrieved from the Cluster Active Archive (CAA), and we thank the FGM PI Elizabeth Lucek for agreeing to distribute the data through CAA, as well as Harri Laakso and team for maintaining the system. The Geotail and Wind magnetic field instrument PIs S. Kokubun and R. P. Lepping are thanked for agreeing to distribute the data freely through the CDAWeb interface, and NASA is thanked for maintaining this great interface. ACE spacecraft recordings are retrieved from the ACE homepage (http://www.srl.caltech.edu/ACE/). We thank the ACE MAG and SWEPAM PIs C. W. Smith and D. J. McComas for distributing the Level 2 data freely in the internet. The research leading to these results has received funding from the European Research Council under the European Community's Seventh Framework Programme (FP7/2007-2013)/ERC Starting Grant agreement 200141-QuESpace. The work of MP is supported by the Academy of Finland. SEM and ML are funded by STFC grant ST/H002480/1.

[42] Philippa Browning thanks the reviewers for their assistance in evaluating this paper.

References

Akasofu, S.-I. (1981), Energy coupling between the solar wind and the magnetosphere, *Space Sci. Rev.*, *28*, 121–190

Axford, W. I., and C. O. Hines (1961) A unifying theory of high-latitude geophysical phenomena and geomagnetic storms, *Can. J. Phys.*, *39*, 1433–1464.

Balogh, A., et al. (2001), The Cluster Magnetic Field Investigation: Overview of in-flight performance and initial results, *Ann. Geophys.*, *19*, 1207–1217.

Cai, D., W. Tao, X. Yan, B. Lembege, and K.-I. Nishikawa (2009), Bifurcation and hysteresis of the magnetospheric structure with a varying southward IMF: Field topology and global three-dimensional full particle simulations, *J. Geophys. Res.*, *114*, A12210, doi:10.1029/2007JA012863.

Cooling, B. M. A., C. J. Owen, and S. J. Schwartz (2001), Role of the magnetosheath flow in determining the motion of open flux tubes, *J. Geophys. Res.*, *106*, 18,764–18,775, doi:10.1029/2000JA000455.

Dungey, J. W. (1961), Interplanetary field and the auroral zones, *Phys. Res. Lett.*, *6*, 47–48.

Janhunen, P. (1996), GUMICS-3: A global ionosphere-magnetosphere coupling simulation with high ionospheric resolution, in Proceedings of Environmental Modelling for Space-Based Applications, 18–20 Sep 1996, Eur. Space Agency Spec. Publ., ESA SP-392.

Kaymaz, Z., G. Siscoe, and J. G. Luhmann (1992), IMF draping around the geotail: IMP 8 observations, *Geophys. Res. Lett.*, *19*, 829–832, doi:10.1029/92GL00403.

Kokubun, S., T. Yamamoto, M. H. Acuna, K. Hayashi, K. Shiokawa, and H. Kawano (1994), The Geotail magnetic field experiment, *J. Geomagn. Geoelectr.*, *46*, 7–21.

Laitinen, T. V., M. Palmroth, T. I. Pulkkinen, P. Janhunen, and H. E. J. Koskinen (2007), Continuous reconnection line and pressure? dependent energy conversion on the magnetopause in a global MHD model, *J. Geophys. Res.*, *112*, A11201, doi:10.1029/2007JA012352.

Lepping, R. P., et al. (1995), The Wind magnetic field investigation, *Space Sci. Rev.*, *71*, 207–229.

Lundin, R., and D. S. Evans (1985), Boundary layer plasmas as a source for high-latitude, early afternoon, auroral arcs, *Planet. Space Sci.*, *33*, 1389–1406.

McPherron, R. L. (1991), Physical processes producing magnetospheric substorms and magnetic storms, in *Geomagnetism*, Vol. 4, pp. 593–739, edited by J. Jacobs, Academic Press Ltd., London, U. K.

McPherron, R. L., and D. N. Baker (1993), Factors influencing the intensity of magnetospheric substorms, *J. Atmos. Terr. Phys.*, *55*, 1091–1122.

McPherron, R. L., D. N. Baker, L. F. Bargatze, C. R. Clauer, and R. E. Holzer (1988), IMF control of geomagnetic activity, *Adv. Space Res.*, *8*, 71–86.

Milan, S. E., G. Provan, and B. Hubert (2007), Magnetic flux transport in the Dungey cycle: A survey of dayside and nightside reconnection rates, *J. Geophys. Res.*, *112*, A01209, doi:10.1029/2006JA011642.

Milan, S. E., A. Grocott, C. Forsyth, S. M. Imber, P. D. Boakes, and B. Hubert (2009), A superposed epoch analysis of auroral evolution during substorm growth, onset and recovery: Open magnetic flux control of substorm intensity, *Ann. Geophys.*, *27*, 659–668.

Newell, P. T., T. Sotirelis, K. Liou, C.-I. Meng, and F. J. Rich (2007), A nearly universal solar wind-magnetosphere coupling function inferred from 10 magnetospheric state variables, *J. Geophys. Res.*, *112*, A01206, doi:10.1029/2006JA012015.

Palmroth, M., T. I. Pulkkinen, P. Janhunen, and C.-C. Wu (2003), Stormtime energy transfer in global MHD simulation, *J. Geophys. Res.*, *108* (A1), 1048, doi:10.1029/2002JA009446.

Palmroth, M., P. Janhunen, T. I. Pulkkinen, and H. E. J. Koskinen (2004), Ionospheric energy input as a function of solar wind parameters: Global MHD simulation results, *Ann. Geophys.*, *22*, 549–566.

Palmroth, M., T. V. Laitinen, and T. I. Pulkkinen (2006a), Magnetopause energy and mass transfer: Results from a global MHD simulation, *Ann. Geophys.*, *24*, 3467–3480.

Palmroth, M., P. Janhunen, and T. I. Pulkkinen (2006b), Hysteresis in solar wind power input to the magnetosphere, *Geophys. Res. Lett.*, *33*, L03107, doi:10.1029/2005GL025188.

Papadopoulos, K., C. Goodrich, M. Wiltberger, R. Lopez, and J. G. Lyon (1999), The physics of substorms as revealed by the ISTP, *Phys. Chem. Earth*, *24*, 189–202.

Raeder, J. (2003), Global magnetohydrodynamics: A tutorial, in *Space Plasma Simulation*, edited by J. Buechner, C. T. Dum, and M. Scholer, Lecture Notes in Physics, vol. 615, Springer-Verlag, Heidelberg, Germany.

Reiff, P. H., R. W. Spiro, and T. W. Hill (1981), Dependence of polar cap potential on interplanetary parameters, *J. Geophys. Res.*, *86*, 7639–7648, doi:10.1029/JA086iA09p07639.

Rosenqvist, L., H. J. Opgenoorth, L. Rastaetter, A. Vaivads, and I. Dandouras (2008), Comparison of local energy conversion estimates from Cluster with global MHD simulations, *Geophys. Res. Lett.*, *35*, L21104, doi:10.1029/2008GL035854.

Rostoker, G., S.-I. Akasofu, W. Baumjohann, Y. Kamide, and R. L. McPherron (1987), The roles of direct input of energy from the solar wind and unloading of stored magnetotail energy in driving magnetospheric substorms, *Space Sci. Rev.*, *46*, 93–111.

Shue, J.-H., J. K. Chao, H. C. Fu, C. T. Russell, P. Song, K. K. Khurana, and H. J. Singer (1997), A new functional form to study the solar wind control of the magnetopause size and shape, *J. Geophys. Res.*, *102*(A5), 9497–9511, doi:10.1029/97JA00196.

Shue, J.-H., et al. (1998), Magnetopause location under extreme solar wind conditions, *J. Geophys. Res.*, *103*, 17,691–17,700, doi:10.1029/98JA01103.

Shukhtina, M. A., E. I. Gordeev, and V. A. Sergeev (2009), Time-varying magnetotail magnetic flux calculation: A test of the method, *Ann. Geophys.*, *27*, 1583–1591.

Siscoe, G. L., and W. D. Cummings (1969), On the cause of geomagnetic bays, *Planet. Space Sci.*, *17*, 1795–1802.

Tanskanen, E., T. I. Pulkkinen, H. E. J. Koskinen, and J. A. Slavin (2002), Substorm energy budget during low and high solar activity: 1997 and 1999 compared, *J. Geophys. Res.*, *107*(A6), 1086, doi:10.1029/2001JA900153.

P. Janhunen, M. Palmroth, T. I. Pulkkinen, and P. K. Toivanen, Finnish Meteorological Institute, 00101 Helsinki, Finland. (minna.palmroth@fmi.fi)

H. E. J. Koskinen, Department of Physics, University of Helsinki, FIN-00014 Helsinki, Finland. (Hannu.E.Koskinen@helsinki.fi)

M. Lester and S. E. Milan, Department of Physics and Astronomy, University of Leicester, University Rd., Leicester, LE1 7RH, UK.